Journal of Industrial and Engineering Chemistry 108 (2022) 449–455

Contents lists available at ScienceDirect

Journal of Industrial and Engineering Chemistry

journal homepage: www.elsevier.com/locate/jiec

Multifunctional nanofiber membrane with anti-ultraviolet and thermal regulation fabricated by coaxial electrospinning

Shuoshuo Wang [a], Wubin Chen [a], Lina Wang [a], Juming Yao [a], Guocheng Zhu [a], Baochun Guo [b], Jiri Militky [c], Mohanapriya Venkataraman [c], Ming Zhang [a,*]

[a] National Engineering Lab for Textile Fiber Materials and Processing Technology, Zhejiang Sci-Tech University, Hangzhou 310018, China
[b] Department of Polymer Materials and Engineering, South China University of Technology, Guangzhou 510640, China
[c] Department of Material Engineering, Faculty of Textile Engineering, Technical University of Liberec, Czech Republic

ARTICLE INFO

Article history:
Received 13 November 2021
Revised 13 January 2022
Accepted 18 January 2022
Available online 26 January 2022

Keywords:
UV protection
Thermal regulation
Core-sheath structure
Multifunctional nanofibers

ABSTRACT

Ultraviolet radiation is extremely harmful to humans and often occurs in high-temperature weather. The development of intelligent textiles based on UV protection and thermal regulation is paramount. In this research, we use coaxial electrospinning technology to prepare anti-ultraviolet smart thermo-regulating nanofiber membranes. The zinc oxide (ZnO) and octadecane were incorporated into nanofibers with the polyacrylonitrile (PAN)/ZnO as sheath and the octadecane as core successfully. The composite nanofibers have excellent comprehensive properties, the highest melting enthalpy is 111.38 J/g, and the UPF value is 86.21. This multifunctional nanofiber membrane has broad prospects in outdoor products, electronic component protection, and military products.
© 2022 The Korean Society of Industrial and Engineering Chemistry. Published by Elsevier B.V. All rights reserved.

Introduction

In recent years, with the destruction of the ozone layer, more ultraviolet (UV) rays have been irradiated to the ground [1–3]. Excessive exposure to UV radiation not only accelerates the photodegradation of organic materials but also harms the human body, causing DNA damage or carcinogenesis [4–8]. Protecting human skin and the environment from UV damage has become a worldwide issue [9,10]. Therefore, different textiles with anti-UV functions, such as curtains, sun-proof clothing, and tents, have attracted people's attention [11].

Generally, the addition of UV absorbers and shielding agents can achieve high anti- UV properties of materials [12,13]. Muzaffar et al. used the pad dry cure technique to finish nano-chitosan-polyurethane dispersion on polyester-cotton fabrics to enhance UV resistance [14]. Zhou et al. loaded titanium dioxide on cotton fabric in situ for modification [15]. Although these methods can improve the anti-UV properties of fabrics, some new problems have arisen, such as complicated steps, uneven dispersion of functional fillers, and poor stability [1,16]. The above troubles can be avoided by blending polymers and various additives to prepare nanofibers through electrospinning technology [17,18]. The obtained composite nanofiber has advantages of large specific surface area, high porosity, and uniform dispersion of functional fillers [19,20]. Therefore, the filler has a larger contact area with UV rays, so the UV-shielding properties of nanofiber membranes are excellent [21]. Commonly used UV absorbers are divided into two types: inorganic and organic. Although organic UV absorbers can effectively improve the UV shielding performance, they are easily decomposed when exposed to UV light for a long time. In contrast, inorganic absorbents overcome the above limitation [22–24]. Zinc oxide (ZnO) nanoparticles are considered the most effective UV absorber, and they also have antibacterial and sensing properties [25–28].

In daily life, high-intensity UV radiation often accompanies high-temperature weather. For human comfort, clothing should also have the function of regulating the temperature [29–31]. Unfortunately, there is no report on UV-proof membranes with thermo-regulation functions so far. Therefore, the development of such intelligent membranes is of great significance. The application of this kind of nanofibers in fabrics brings good protection for people or electronic components who are often outdoors. Integrating functional materials that respond to environmental temperature changes into textiles is a research hotspot all the time [32,33]. Currently, phase change materials (PCMs) have attracted the attention of researchers due to their excellent performance in storing and converting energy [34–36]. PCMs can easily store or

* Corresponding author.
E-mail address: zhangming@zstu.edu.cn (M. Zhang).

https://doi.org/10.1016/j.jiec.2022.01.022
1226-086X/© 2022 The Korean Society of Industrial and Engineering Chemistry. Published by Elsevier B.V. All rights reserved.

release thermal energy to maintain a constant temperature. Because of this feature, it has a good application prospect in apparel [37–39]. However, the leakage problem during the phase change process limits the practical application of PCMs [40,41]. Coaxial electrospinning technology has unique advantages in solving this problem. Because of the use of coaxially arranged spinnerets, nanofibers with a core-sheath structure can be directly produced [42,43]. Benefiting from the protection of the polymer sheath, the stability of the PCMs is greatly improved. For example, Lu et al. prepared paraffin-loaded nanofibers [44]. Moreover, this method can easily integrate anti-ultraviolet and intelligent thermo-regulation functions into the fabric. With the emergence of coaxial electrospinning technology, the development of multifunctional nanofibers has more options [45].

Herein, we prepared UV-resistant nanofiber membranes with intelligent temperature regulation performance using the coaxial electrospinning method. Polyacrylonitrile (PAN) was used as the polymer substrate because it has the advantages of good mechanical properties, stable thermal properties, and excellent spinnability [46]. The UV absorber is ZnO nanoparticles. The selected PCM is octadecane, which has stable thermal performance, high latent heat, and low price [47]. Explore how ZnO is embedded in PAN nanofibers to prepare composite nanofibers with excellent UV protection properties. In addition, loading octadecane into the nanofibers imparts its thermal regulation properties. The unique core-sheath structure prevents PCMs from leaking so that the fiber membrane has stable thermal performance. In general, we have successfully integrated UV protection and temperature regulation properties into PAN nanofiber membranes. It reveals the promising application of the multifunctional membrane in the protection of sunscreen clothing, outdoor products, and electronic components.

Experimental

Materials

Polyacrylonitrile (PAN, M_w = 150000) was bought from Sinopec Shanghai Petrochemical Co., Ltd. Zinc oxide (ZnO, 99.9%, 30 ± 10 nm), Octadecane (99%, the melting temperature is around 28 °C) and Petroleum ether (AR, bp 90–120 °C) were purchased from Aladdin Chemistry Co., Ltd. N, N-dimethylformamide (DMF) was purchased from Hangzhou Gaojing Fine Chemical Industry Co., Ltd.

Fabrication of the nanofiber membrane

The PAN solution was obtained by dissolving PAN in DMF at a concentration of 14 wt% and stirring at ambient temperature for 6 hours. To obtain the PAN/ZnO composite sheath, ZnO was added to DMF at different concentrations of 1, 3, 5, and 7 wt%, respectively, and sonicated for 1 hour. Then 14 wt% PAN was added and stirred for 12 hours at ambient temperature and then sonicated for 1 hour. The octadecane needs to be heated to melt before electrospinning. The outer diameter of the uniaxial needle used is 1.2 mm. The coaxial stainless-steel needle consists of an inner needle (with an inner diameter of 0.41 mm and an outer diameter of 0.72 mm) and an outer needle (with an inner diameter of 1.01 mm and an outer diameter of 1.49 mm). Put the sheath and core solutions into two 10 mL plastic syringes and connect them to different needles. The feed rate of sheath solutions was 0.6 mL/h, and the core solutions feed rate was varied from 0.05 to 0.25 mL/h. Apply a positive voltage of 25 kV to the needle. The distance from the tip to the collector is 15 cm. The temperature and humidity during spinning were controlled at 45 °C and 45%, respectively.

Characterizations

The morphology of the nanofibers was observed using a field emission scanning electron microscope (FE-SEM, ULTRA55, Zeiss) at a 3 kV acceleration voltage. All samples need to be plated with a thin layer of gold before observation with the FE-SEM. Use ImageJ software to randomly measure the diameter of 50 fibers, and calculate the average diameter and deviation. The transmission electron microscope (TEM, JEM-1400, JOEL) at an acceleration voltage of 200 kV was used to characterize the core-sheath structure of nanofibers. The TEM samples were prepared by depositing nanofibers on a 400-mesh carbon-coated Cu grid, and need to be immersed in petroleum ether for 24 hours to remove the inner core layer before observation. UV/Vis/NIR spectrophotometer (UH4150) was used to measure the UV transmittance of fabrics. The UV protection factor (UPF) of electrospun nanofiber membranes can be expressed as:

$$\mathrm{UPF} = \frac{\int_{\lambda=290}^{\lambda=400} E(\lambda).S(\lambda).d\lambda}{\int_{\lambda=290}^{\lambda=400} E(\lambda).S(\lambda).T(\lambda).d\lambda}, \tag{1}$$

where E(λ) is the relative erythema spectral influence, S(λ) is the solar spectral irradiance, T(λ) is the spectral transmittance of the fabric, λ is the ultraviolet wavelength, and dλ is the wavelength difference. The thermal performance of PAN@Octa and PAN/$ZnO_{7\%}$@Octa (PAN@Octa represents core-sheath structured, with PAN sheath and octadecane core nanofibers; 7% means that the ZnO concentration is 7 wt%) was characterized by differential scanning calorimetry (DSC, Q2000). The sample was heated from 0 to 45 °C and then cooled from 45 to 0 °C at a rate of 10 K/min. This test was carried out in a stream of nitrogen. Perform thermogravimetric analysis (L81/1750TGA, LINSEIS Company, Germany) to study the thermal stability and decomposition performance of samples. The mechanical properties of nanofiber membranes are measured by the multifunctional mechanical tester (KES-G1). Cut the tested samples into pieces of 0.5 × 2 cm, and measure the thickness separately.

Results and discussion

Fig. 1 shows the morphology of as-prepared nanofibers. It can be seen from the figure that PAN nanofibers exhibit straight, randomly oriented cylindrical structures with a smooth surface. The ZnO nanoparticles are irregular blocky structures, mostly stacked together. Adding ZnO to the PAN solution changed the fiber morphology. While the ZnO concentration was 1 wt%, some small protrusions can be observed on the fiber surface, indicating that the ZnO was successfully embedded. With the increase of ZnO addition, the fiber has more protuberances. ZnO almost distributes the whole nanofibers under a concentration of 7 wt%, which shows that it is well dispersed. The corresponding TEM image is shown in Fig. S1, which is more intuitive. The characteristic elements zinc and oxygen in the EDS results (Fig. 2a) of PAN/ZnO composite nanofibers belong to ZnO. Fig. 2b summarizes the average diameter and deviation of PAN/ZnO nanofibers. The increase in the ZnO concentration results in a larger average diameter and deviation. This tendency of change is attributed to the enlargement of the electrospinning solution viscosity [44].

UV radiation usually refers to waves with lengths of 100–400 nm, which is divided into three types: ultraviolet A (UVA), ultraviolet B (UVB), and ultraviolet C (UVC). Although the ozone layer almost completely absorbs UVC (200–280 nm), UVA (320–400 nm) and UVB (280–320 nm) still have serious radiation hazards. Therefore, UV protection materials mainly block UVA and UVB [48,49]. Herein, ZnO was added to impart long-lasting UV resistance to the PAN membrane. The UV-blocking mechanism of PAN/ZnO nanofiber membranes was studied by UV transmission

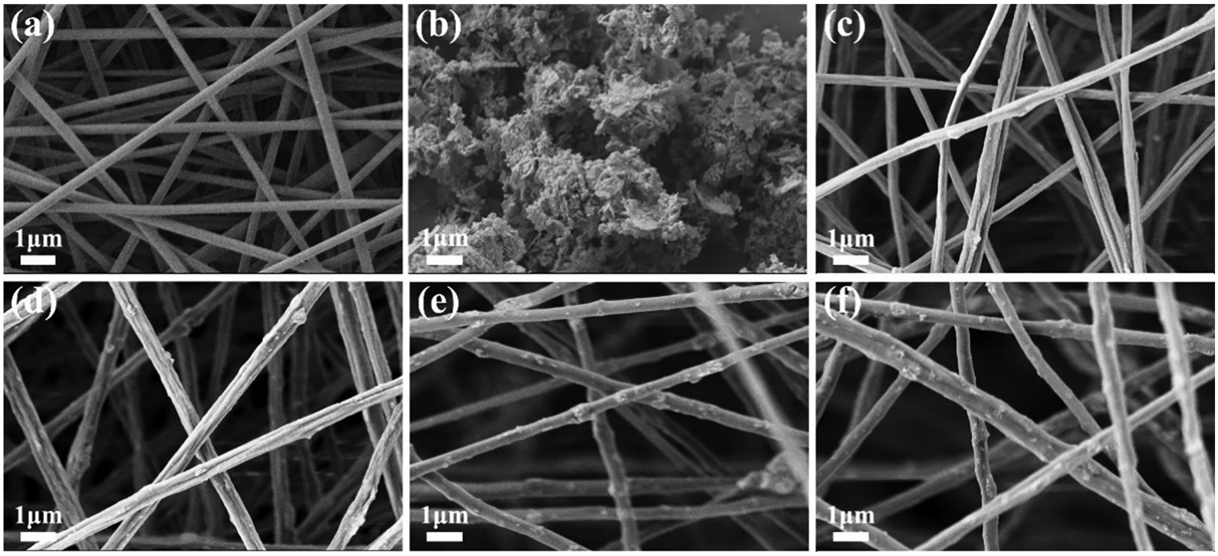

Fig. 1. The FE-SEM images of (a) PAN nanofibers, (b) ZnO, and the electrospun nanofibers with ZnO concentration (wt%) of (c) 1%, (d) 3%, (e) 5%, and (f) 7%.

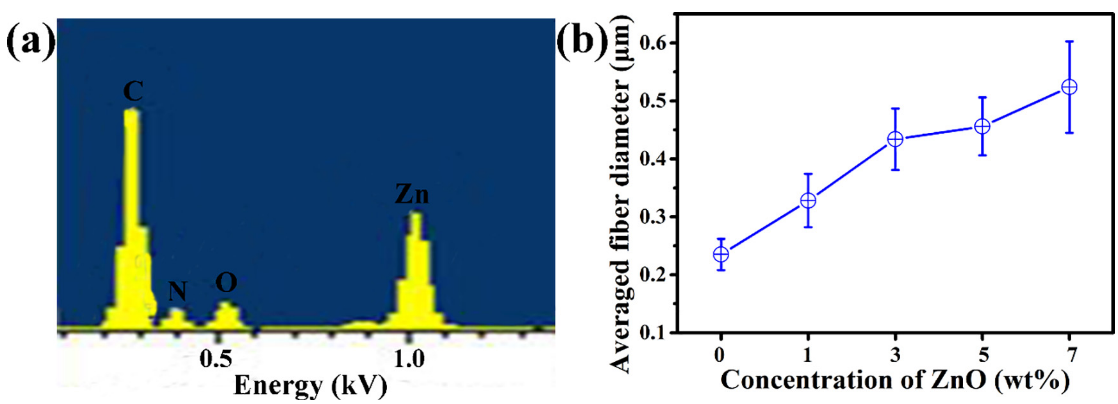

Fig. 2. (a) EDS curve of PAN/ZnO nanofibers, (b) the average diameters of PAN/ZnO nanofibers containing different ZnO concentrations.

and absorption spectroscopy. As shown in Fig. 3a, the UV transmission peak of the neat PAN membrane is obvious. After adding ZnO, the UV transmittance of the PAN membrane decreases, especially in the range of 280–380 nm, which is almost zero. The significant decrease in UV transmittance is attributed to the UV absorption capacity of ZnO.

It can be seen from Fig. 3b that the PAN membrane has virtually no absorption of UV radiation. Conversely, the PAN/ZnO composite nanofiber membranes have broad absorption peaks. The principle of ZnO absorbing UV light is to rely on the electrons in the valence band to accept the energy in the UV light for transition. Applying ZnO to PAN membranes to provide UV protection is efficacious. In addition to the absorption capacity of ZnO, the catadioptric performance of PAN/ZnO membranes is also indispensable. Ultraviolet protection factor (UPF) is one of the primary indicators for evaluating UV shielding performance. The higher the UPF value, the better the UV protection performance. When it is higher than 40, the protection effect is excellent. Fig. 3c is the UPF value of prepared fiber membranes. The UPF value of pure PAN membrane is 7.12, which is almost no UV resistance. As the concentration of ZnO increases, the UPF value enlarges significantly. When the ZnO concentration is 7 wt%, the highest UPF value is 147.04. According to the results of UV absorption, reflection spectra and UPF, it is indicated that the addition of ZnO provides excellent UV shielding performance for PAN membrane due to its UV absorption and reflection functions. Fig. 3d is the anti-UV schematic diagram of PAN/ZnO membranes.

Coaxial electrospinning technology was used to prepare octadecane-loaded core-sheath structure nanofibers. Fig. 4 shows the FE-SEM images of PAN@Octa nanofibers. When octadecane is encapsulated in PAN, PAN@Octa presents almost the same morphology as PAN nanofibers. The surface of PAN@Octa is smooth after soaking in petroleum ether, indicating that octadecane existed inside of the fibers. The morphology of PAN/$ZnO_{7\%}$@Octa (Fig. S2) did not change compared with that before loading octadecane. The average diameter of these nanofibers is 350 nm, which is about 150 nm larger than PAN@Octa nanofibers.

The DSC curve of core-sheath nanofibers and the corresponding summarized values are shown in Fig. 5 and Table 1. During the crystallization process, some curves have two exothermic peaks. Because there are few PCMs encapsulated in the fiber, the supercooling effect is enhanced [50]. When the size of PCMs is small, phase separation is more likely to occur. The $\triangle H_m$ of PAN@Octa nanofibers are 56.21 and 126.39 J/g at the core feed rate of 0.05 and 0.25 mL/h, respectively. It shows that higher core feed rates can lead to higher latent heat values because the polymer can encapsulate more PCMs. However, the latent heat cannot increase indefinitely and gradually reach a plateau, which is the highest encapsulation rate under this condition. The latent heat of PAN/$ZnO_{7\%}$@Octa is smaller than PAN@Octa. Due to the thicker sheath

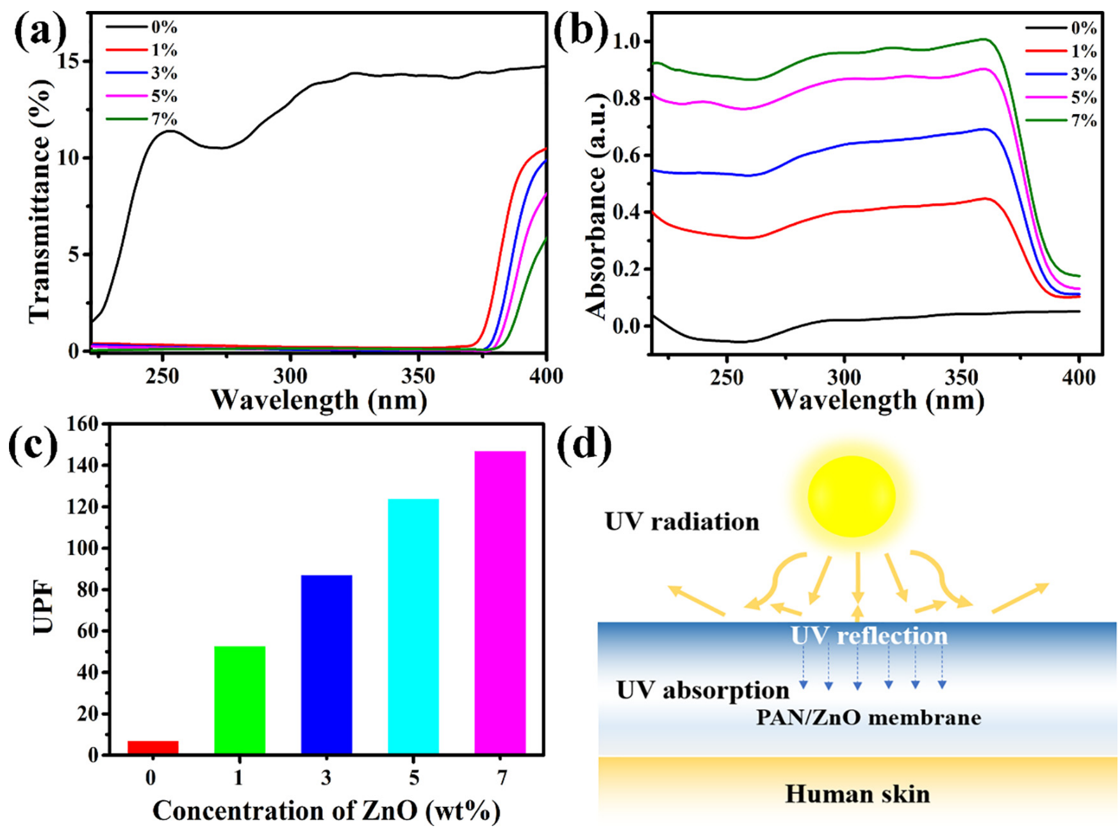

Fig. 3. Comprehensive performance of PAN/ZnO nanofiber membranes with different ZnO concentrations: (a) UV transmittance spectra, (b) UV absorption spectra, (c) UPF. (d) Schematic of UV resistance, including reflection and absorption.

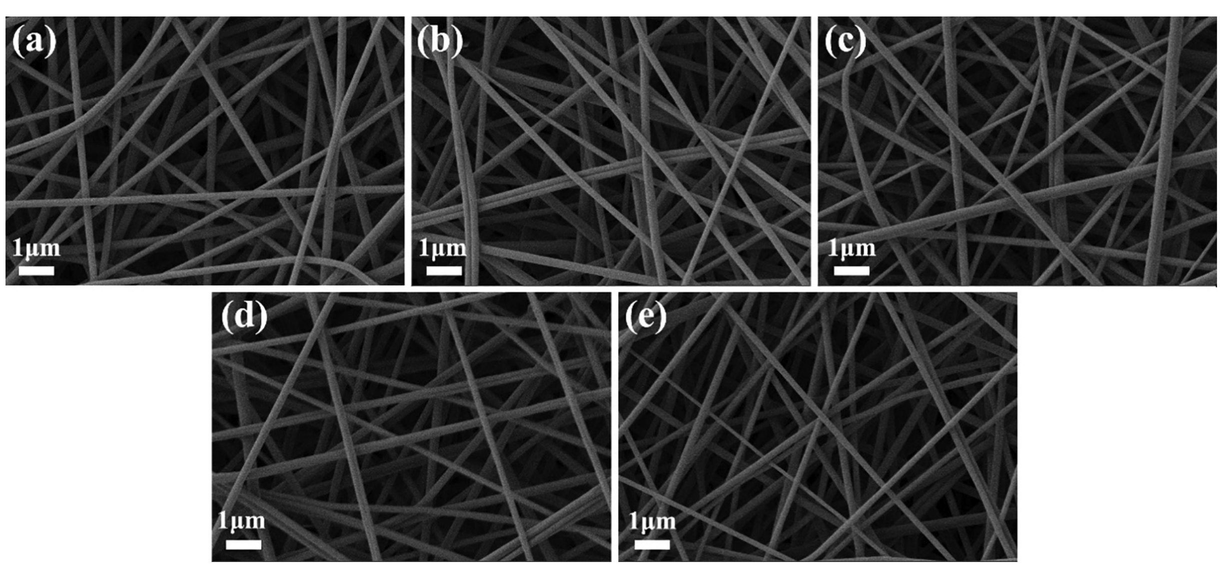

Fig. 4. The FE-SEM images of PAN@Octa nanofibers with different core feed rates: (a) 0.05 m/L, (b) 0.10 m/L, (c) 0.15 m/L, (d) 0.20 m/L, (e) 0.25 m/L.

of PAN/$ZnO_{7\%}$@Octa, the proportion of polymer components is higher. The polymer only adds weight without phase change, so the latent heat of the fiber is lower. It can be seen from the DSC curves that PAN/$ZnO_{7\%}$@Octa has a broad peak during melting and crystallization processes, and the melting temperature is also higher, which is attributed to the thicker sheath. The loading amount of octadecane in composite nanofibers can be calculated by the following formula: Encapsulation ratio (%) = $\frac{\Delta H_{m,\ PCM/Sheath}}{\Delta H_{m,\ PCM}} \times$ 100%, (2) where $\triangle H_{m,PCM/Sheath}$ and $\triangle H_{m,PCM}$ represent the melting enthalpy of composite nanofibers and PCM. The highest latent heat value of PAN/$ZnO_{7\%}$@Octa is 111.38 J/g, and the calculated encapsulation amount of octadecane is 43.67%.

After loading octadecane, the anti- UV performance of composite nanofiber membranes decreased. As displayed in Fig. 6a, all UV transmission spectra have shifted upward. It shows that the more octadecane encapsulated in the fiber, the worse the UV protection performance. The variety in the UV absorption spectrum can

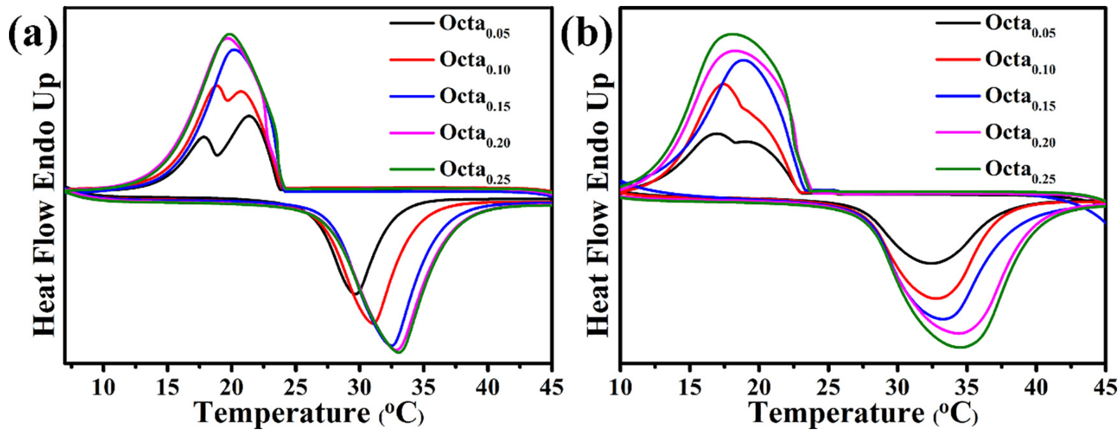

Fig. 5. The DSC curves of samples with different sheath: (a) PAN, (b) PAN/$ZnO_{7\%}$.

Table 1
The DSC analyses data of samples and octadecane.

Samples	Feed rate (mL/h)	T_m (°C)	△H_m (J/g)	T_c (°C)	△H_c (J/g)
PAN@Octa	0.05	29.67	56.21	21.34	54.81
	0.10	31.03	83.07	18.85	81.37
	0.15	32.51	107.33	20.22	103.45
	0.20	32.84	121.93	19.66	117.58
	0.25	33.04	126.39	19.84	123.62
PAN/$ZnO_{7\%}$@Octa	0.05	32.40	42.89	18.94	40.24
	0.10	32.85	60.91	18.40	59.64
	0.15	33.21	79.82	18.99	76.16
	0.20	34.37	93.75	18.24	91.40
	0.25	34.43	111.38	18.12	109.41
Octadecane		28.36	255.03	19.76	251.33

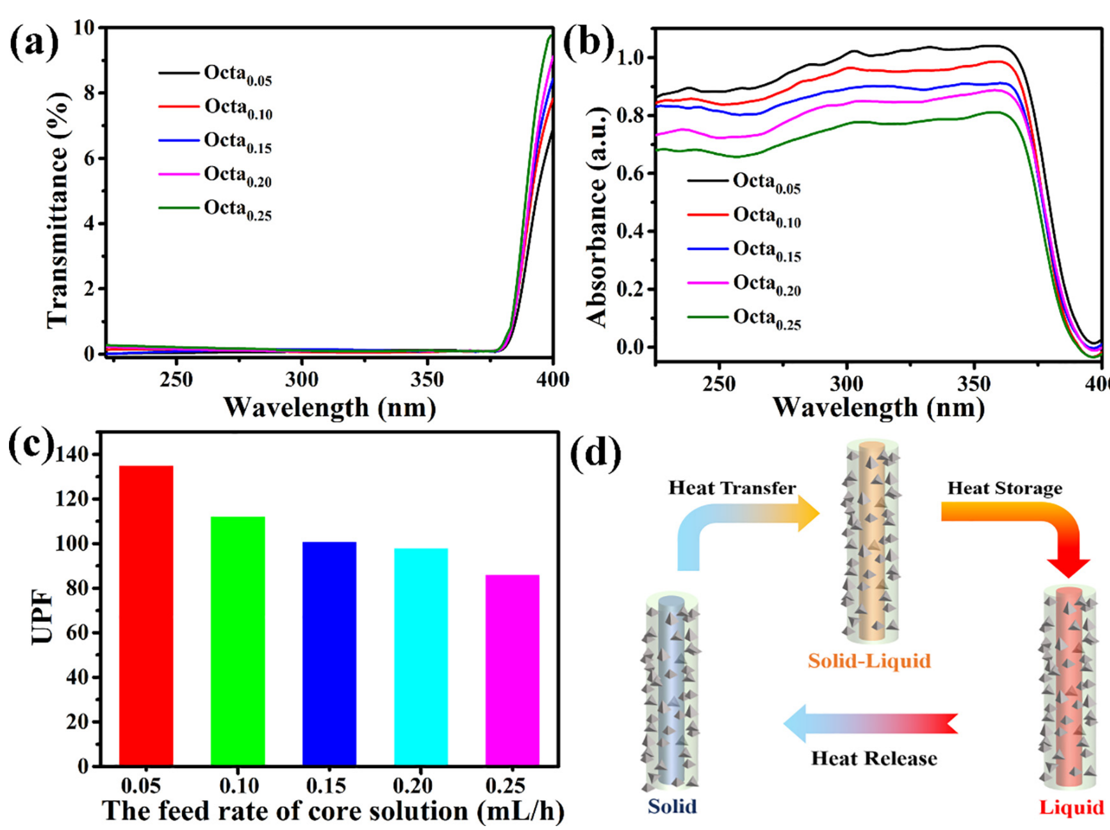

Fig. 6. Comprehensive performance of PAN/$ZnO_{7\%}$@Octa nanofiber membranes with different core feed rate: (a) UV transmittance spectra, (b) UV absorption spectra, (c) UPF. (d) Heat transfer process of the PAN/$ZnO_{7\%}$@Octa nanofibers.

explain the increase in UV transmittance. Fig. 6b indicates that as the core feed rate increases, the UV absorption capacity of PAN/$ZnO_{7\%}$@Octa decreases. Therefore, more UV rays pass through the nanofiber membrane. The UPF (Fig. 6c) is used to evaluate the UV protection level of PAN/$ZnO_{7\%}$@Octa. When the core feed rate is 0.05 mL/h, the UPF value drops slightly to 135.14. As the core feed rate increases to 0.25 mL/h, the UPF value becomes 86.21. Although the UPF value of PAN/$ZnO_{7\%}$@Octa is reduced, compared with other studies, its UV protection performance is still excellent. The heat transfer process of core-sheath nanofibers is shown in Fig. 6d. The octadecane-loaded thermo-regulated membranes can adjust the temperature by releasing or absorbing heat when the octadecane changes the phases from liquid to solid or solid to liquid.

Fig. 7 is the TEM images of octadecane-loaded composite nanofibers prepared by coaxial electrospinning. The polymer completely covers the octadecane to form an ideal core-sheath structure. Due to the influence of sheath solution viscosity, PAN/$ZnO_{7\%}$@$Octa_{0.25}$ (0.25 means that the core feed rate is 0.25 mL/h) is thicker, consistent with the average diameter obtained above. In addition, Fig. 7b shows that ZnO distributed in the nanofibers obvious. There are still some agglomeration phenomena in ZnO nanoparticles. Further research is needed to improve its dispersion. The nanofibers are subjected to a thermal cycle test, and the morphology and DSC curve obtained are shown in Fig. S3. It can be seen from the figure that there is almost no change in the morphology and property of the fiber, indicating that its performance is stable. Fig. 8 shows the TGA curves of octadecane and composite fibers. The octadecane is completely decomposed at about 250 °C. The decomposition of PAN/$ZnO_{7\%}$@$Octa_{0.25}$ is in two stages. The first stage is due to the thermal decomposition of octadecane, and the loss of mass is about 41%. This value is the load of octadecane, which is consistent with the value calculated from the melting enthalpy. The second stage is the decomposition of PAN. The decomposition temperature of octadecane increases after encapsulation. It shows that the core-sheath structure can improve the thermal stability of PCMs to achieve better practical applications.

The stress–strain curves are shown in Fig. 9, which illustrates the influence of ZnO and octadecane on the mechanical properties of nanofiber membranes. After adding ZnO to the PAN solution, the breaking elongation of the nanofibers hardly changed, and the mechanical strength was reduced. It can be explained that ZnO destroys the connections inside nanofibers [1]. When the nanofibers are loaded with octadecane, the breaking elongation of the fiber drops a lot, and the mechanical strength is slightly reduced. Since the solid PCM is brittle, it weakens the mechanical properties of fibers [47].

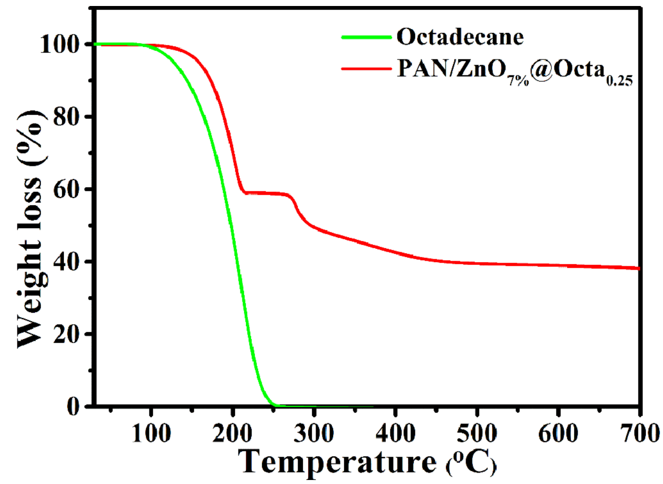

Fig. 8. The TGA curves of octadecane and PAN/$ZnO_{7\%}$@$Octa_{0.25}$.

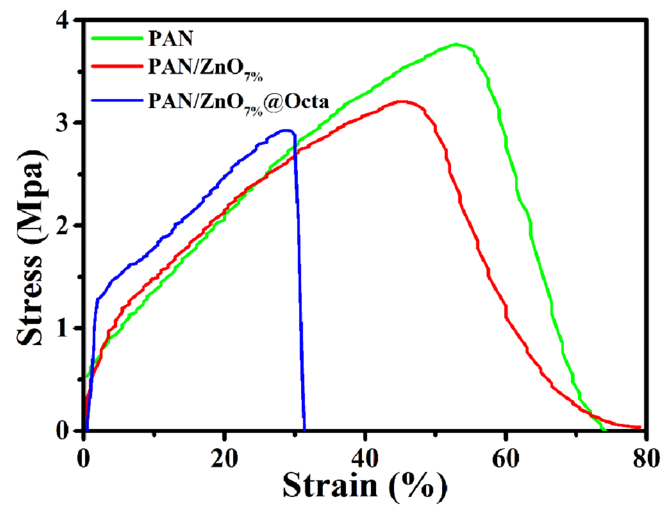

Fig. 9. The stress–strain curves of nanofiber membranes prepared under different experimental conditions.

Conclusions

In summary, we fabricated multifunctional nanofiber membrane with UV protection and thermal regulation through coaxial electrospinning technology. The ZnO nanoparticles are incorpo-

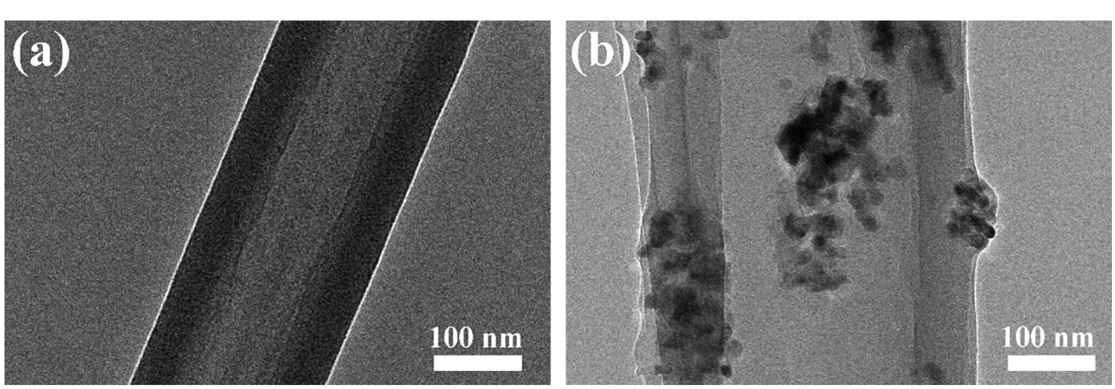

Fig. 7. The TEM images of (a) PAN@$Octa_{0.25}$, (b) PAN/$ZnO_{7\%}$@$Octa_{0.25}$.

rated into nanofibers to endow the fabric with stable and excellent UV resistance. The TEM images show that the polymer successfully encapsulated the octadecane and formed a visible core–shell structure. Under the protection of the polymer sheath, the thermal stability of the PCM is improved. Although the UV resistance of textiles after loading with octadecane decreases, the comprehensive performance of the composite nanofiber membrane is still excellent. Hence, this work provides valuable support for the research of multifunctional nanofibers.

Declaration of Competing Interest

The authors declare that they have no known competing financial interests or personal relationships that could have appeared to influence the work reported in this paper.

Acknowledgement

The authors acknowledge financial support supported by China Education Association for International Exchange (project No. 202020).

Appendix A. Supplementary data

Supplementary data to this article can be found online at https://doi.org/10.1016/j.jiec.2022.01.022.

References

[1] K. Liu, L. Deng, T. Zhang, K. Shen, X. Wang, Ind. Eng. Chem. Res. 59 (2020) 4447–4458.
[2] R.M. Lucas, S. Yazar, A.R. Young, M. Norval, F.R. de Gruijl, Y. Takizawa, L.E. Rhodes, C.A. Sinclair, R.E. Neale, Photochem. Photobiol. Sci. 18 (2019) 641–680.
[3] A.M. El-Toni, S. Yin, T. Sato, T. Ghannam, M. Al-Hoshan, M. Al-Salhi, J. Alloy. Compd. 508 (2010) L1–L4.
[4] S.Y.H. Abdalkarim, H.-Y. Yu, C. Wang, L. Yang, Y. Guan, L. Huang, J. Yao, ACS Appl. Bio Mater. 1 (2018) 714–727.
[5] X. Chen, D. Hu, Z. Zhang, W. Ma, J. Alloy. Compd. 811 (2019).
[6] H. Bian, L. Chen, M. Dong, L. Wang, R. Wang, X. Zhou, C. Wu, X. Wang, X. Ji, H. Dai, Int. J. Biol. Macromolecules 166 (2021) 1578–1585.
[7] H. Sadeghifar, R.A. Venditti, J.S. Jur, R.E. Gorga, J.J. Pawlak, ACS Sustainable Chem. Eng. 5 (2016) 625–631.
[8] N.A. Ibrahim, H.M. Khalil, B.M. Eid, J. Cleaner Prod. 92 (2015) 187–195.
[9] J.Y. Huang, S.H. Li, M.Z. Ge, L.N. Wang, T.L. Xing, G.Q. Chen, X.F. Liu, S.S. Al-Deyab, K.Q. Zhang, T. Chen, Y.K. Lai, J. Mater. Chem. A 3 (2015) 2825–2832.
[10] W. Ma, Y. Ding, M. Zhang, S. Gao, Y. Li, C. Huang, G. Fu, J. Hazard. Mater. 384 (2020).
[11] H. Palak, B. Aktürk, B.K. Kayaoğlu, İ. Göcek, J. Ind. Text. (2021), 152808372110208.
[12] X. Dong, S. Gao, J. Huang, S. Li, T. Zhu, Y. Cheng, Y. Zhao, Z. Chen, Y. Lai, J. Mater. Chem. A 7 (2019) 2122–2128.
[13] Q. Yang, L. Zhao, H. Yu, Q. Min, C. Chen, D. Zhou, Yu Xue, J. Qiu, B. Li, X. Xu, J. Alloy. Compd. 784 (2019) 535–540.
[14] S. Muzaffar, M. Abbas, U.H. Siddiqua, M. Arshad, A. Tufail, M. Ahsan, S.A. Alissa, S.A. Abubshait, H.A. Abubshait, M. Iqbal, J. Mater. Res. Technol. 11 (2021) 946–956.
[15] W. Zhou, Y.-Y. Zhang, Y.-D. Shi, Fibers Polym. 18 (2017) 1073–1078.
[16] X. Wang, X. Chen, S. Cowling, L. Wang, X. Liu, Adv. Mater. Interfaces 6 (2019) 1900564.
[17] Y.-Y. Chen, C.-C. Kuo, B.-Y. Chen, P.-C. Chiu, P.-C. Tsai, J. Polym. Sci. Part B: Polym. Phys. 53 (2015) 262–269.
[18] K. Nasouri, Polym. Compos. 40 (2019) 3325–3332.
[19] A. Gholamhosseini, K. Nasouri, A.M. Shoushtari, F. Mirgoli, Fibers Polym. 21 (2020) 1704–1712.
[20] N. Neamjan, W. Sricharussin, P. Threepopnatkul, J. Nanosci. Nanotechnol. 12 (2012) 525–530.
[21] M. Shabbir, F. Mohammad, Appl. Nanosci. 8 (2018) 545–555.
[22] M.Z. Khan, V. Baheti, M. Ashraf, T. Hussain, A. Ali, A. Javid, A. Rehman, Fibers Polym. 19 (2018) 1647–1654.
[23] A. Khan, A. Nazir, A. Rehman, M. Naveed, M. Ashraf, K. Iqbal, A. Basit, H.S. Maqsood, Int. J. Clothing Sci. Technol. 32 (2020) 869–890.
[24] M. Mahmoudifard, M. Safi, J. Text. Inst. 103 (2012) 893–899.
[25] X.-S. Hu, Y. Shen, L.-H. Xu, L.-M. Wang, Y.-J. Xing, J. Alloy. Compd. 674 (2016) 289–294.
[26] D. Lee, D. Park, K. Shin, H.M. Seo, H. Lee, Y. Choi, J.W. Kim, J. Ind. Eng. Chem. 96 (2021) 219–225.
[27] N.A. Ibrahim, B.M. Eid, H.M. Khalil, A.A. Almetwally, Appl. Surf. Sci. 448 (2018) 95–103.
[28] N.A. Ibrahim, A.A. Nada, B.M. Eid, M. Al-Moghazy, A.G. Hassabo, N.Y. Abou-Zeid, Adv. Natural Sci.: Nanosci. Nanotechnol. 9 (2018), 035014.
[29] C. Chen, L. Wang, Y. Huang, Polymer 48 (2007) 5202–5207.
[30] R. Gupta, S. Kedia, N. Saurakhiya, A. Sharma, A. Ranjan, Sol. Energy Mater. Sol. Cells 157 (2016) 676–685.
[31] F. Haghighat, S.A. Hosseini Ravandi, M.N. Esfahany, A. Valipouri, Z. Zarezade, Appl. Therm. Eng. 161 (2019).
[32] Y. Lu, X. Xiao, J. Fu, C. Huan, S. Qi, Y. Zhan, Y. Zhu, G. Xu, Chem. Eng. J. 355 (2019) 532–539.
[33] A. Babapoor, G. Karimi, M. Khorram, Appl. Therm. Eng. 99 (2016) 1225–1235.
[34] M.K. Rathod, J. Banerjee, Renew. Sustain. Energy Rev. 18 (2013) 246–258.
[35] A. Sarı, C. Alkan, A. Karaipekli, Appl. Energy 87 (2010) 1529–1534.
[36] L. Colla, L. Fedele, S. Mancin, L. Danza, O. Manca, Appl. Therm. Eng. 110 (2017) 584–589.
[37] Y. Wu, C. Chen, Y. Jia, J. Wu, Y. Huang, L. Wang, Appl. Energy 210 (2018) 167–181.
[38] H. Yang, S. Wang, X. Wang, W. Chao, N. Wang, X. Ding, F. Liu, Q. Yu, T. Yang, Z. Yang, J. Li, C. Wang, G. Li, Appl. Energy 261 (2020).
[39] S. Wang, L. Yi, L. Wang, J. Yao, J. Militky, M. Venkataramam, J. Wiener, M. Zhang, Polymer 228 (2021).
[40] Y. Lu, X. Xiao, J. Mo, C. Huan, S. Qi, Y. Zhan, Y. Zhu, G. Xu, Colloids Surf. A: Physicochem. Eng. Aspects 555 (2018) 501–506.
[41] A. Babapoor, G. Karimi, S.I. Golestaneh, M.A. Mezjin, Appl. Therm. Eng. 118 (2017) 398–407.
[42] F. Haghighat, S.A. Hosseini Ravandi, M. Nasr Esfahany, A. Valipouri, J. Mater. Sci. 53 (2017) 4665–4682.
[43] E.C.B. Noyan, E. Onder, N. Sarier, R. Arat, Thermochim. Acta 662 (2018) 135–148.
[44] Y. Lu, X. Xiao, Y. Zhan, C. Huan, S. Qi, H. Cheng, G. Xu, ACS Appl. Mater. Interfaces 10 (2018) 12759–12767.
[45] Y. Lu, X. Xiao, Y. Liu, J. Wang, S. Qi, C. Huan, H. Liu, Y. Zhu, G. Xu, J. Alloy. Compd. 812 (2020).
[46] S. Fang, W. Wang, X. Yu, H. Xu, Y. Zhong, X. Sui, L. Zhang, Z. Mao, Mater. Lett. 143 (2015) 120–123.
[47] L. Yi, Y. Wang, Y. Fang, M. Zhang, J. Yao, L. Wang, J. Marek, RSC Adv. 9 (2019) (1851) 21844–21852.
[48] S.M.M. Kabir, A.K. Dhar, J. Koh, Fibers Polym. 22 (2021) 382–386.
[49] A. Kocić, M. Bizjak, D. Popović, G.B. Poparić, S.B. Stanković, J. Cleaner Prod. 228 (2019) 1229–1237.
[50] E. Zdraveva, J. Fang, B. Mijovic, T. Lin, Ind. Eng. Chem. Res. 54 (2015) 8706–8712.